VISCOELASTIC SIMULATION OF BI-LAYER COEXTRUSION IN A SQUARE DIE: AN ANALYSIS OF VISCOUS ENCAPSULATION

Mahesh Gupta

Michigan Technological University
Houghton, MI 49931

Plastic Flow, LLC
Hancock, MI 49930

Abstract

The Giesekus model is used for viscoelastic simulation of a bi-layer flow in a square die. In contrast to the experimental data reported in the literature, in the present work even with viscoelastic effects included in the simulation, encapsulation of a high viscosity polymer by a lower viscosity polymer could not be captured. Since the viscous encapsulation could not be captured with a purely viscous formulation either, it is concluded that the difference in the wettability and surface tension of the two polymers is probably the major factor resulting in the encapsulation.

Introduction

Coextrusion, which involves simultaneous extrusion of several different polymers through a die, combines the functionalities and benefits of several polymers into a single multi-layered product [1]. Despite this inherent advantage of coextrusion, design of coextrusion dies is difficult because depending upon the rheology of polymers used for coextrusion, the polymers in various layers may get redistributed as they flow through the die such that the distribution of various polymers at the inlet and at the exit of the die may be quite different. In particular, it has been observed in coextrusion experiments that as two polymers with different viscosities flow together, in the region near the die walls the lower viscosity polymer tends to encapsulate the higher viscosity polymer [2]. Because of the undesirable variation in layer thickness caused by the encapsulation, plastic films and sheets are often trimmed at the ends to discard these non-uniform portions.

Unfortunately, the root cause behind the encapsulation phenomena, whether it is caused by the difference in viscosity, or in viscoelasticity, or in some other property of the two polymers, is still not completely understood. Simulations of coextrusion using a purely viscous formulation available in the literature [3], including our earlier work [4], have not been successful in capturing the encapsulation. This may lead one to believe that the encapsulation must be caused by viscoelastic effects, which was supported by some papers [5] on viscoelastic simulation of a bi-layer flow in the literature. In contrast, the simulation results presented in this paper indicate that the encapsulation is not caused by viscoelastic effects. Therefore, at this point we believe that the unbalanced force at the contact line where the two polymers together meet the die wall is the main driving force which results in the observed encapsulation. This unbalanced force at the contact line originates from the difference in the wettability and surface tension of the two polymers.

Viscoelastic Formulation for Polymeric Flow

To capture the viscoelastic behavior of polymers, the Giesekus model (Eqn. 1) [6] was employed in the current work.

$$\tilde{\tau}_i + \lambda_i \overset{\nabla}{\tilde{\tau}}_i + (\alpha_i \lambda_i / \eta_i)\, \tilde{\tau}_i \cdot \tilde{\tau}_i = 2\eta_i \tilde{e} \qquad (1)$$

where $\tilde{\tau}_i$ is the contribution of the i^{th} relaxation time (λ_i) to the viscoelastic stress $\tilde{\tau}_e = \sum_{i=1}^{N} \tilde{\tau}_i$, η_i is the polymeric viscosity of the i^{th} relaxation mode, $\tilde{e} = (\nabla\vec{u} + \nabla\vec{u}^T)/2$ is the strain-rate tensor with $\vec{u}$ being the velocity, and α_i, is an additional material parameter for each relaxation mode which controls the ratio N_2/N_1, with N_1 and N_2 being the first- and the second-normal stress differences, respectively. The triangle on top of $\tilde{\tau}_i$ denotes upper-convected material derivative, which is defined as [6]:

$$\overset{\nabla}{\tilde{\tau}}_i \equiv D\tilde{\tau}_i/Dt - \nabla\vec{u}\cdot\tilde{\tau}_i - \tilde{\tau}_i \cdot \nabla\vec{u}^T \qquad (2)$$

where $D\tilde{\tau}_i/Dt$ is the material derivative of $\tilde{\tau}_i$.

Besides the constitutive equation, simulation of viscoelastic flow requires solving the mass and momentum conservation equations. Assuming a steady, inertia-less, isothermal, incompressible flow with no body force, the conservation equations for momentum and mass are simplified to

$$\nabla \cdot \tilde{\sigma} = 0 \qquad (3)$$

$$\nabla \cdot \vec{u} = 0 \qquad (4)$$

where the total stress, $\tilde{\sigma}$ is given by the following equation

$$\tilde{\sigma} = -p\tilde{\delta} + 2\eta_s \tilde{e} + \sum_{i=1}^{N} \tilde{\tau}_i \qquad (5)$$

with p being the pressure, η_s the solvent viscosity, $\tilde{\delta}$ is the identity tensor, and N is the number of modes in the viscoelastic constitutive equation.

Numerical Scheme for Flow Simulation

To obtain the finite element formulation of the flow problem, in the present work, the standard Galerkin method [7] was used for mass and momentum conservation equations (Eqns. 3 – 5). However, for stability of the numerical scheme, a streamline-upwind-

Petrov-Galerkin (SUPG) method [8] was employed for the Giesekus constitutive equation (Eqn. 1). For additional stability of the numerical scheme the DEVSS method [9] was employed for discretization of the momentum equation (Eqns. 3 and 5). In DEVSS method an elliptic operator $2\eta_a(\tilde{e} - \tilde{e}_a)$ is introduced in the momentum equation, where $\tilde{e}_a$ is a discrete approximation of the strain-rate tensor $\tilde{e}$, and $\eta_a = \sum_{i=1}^{N} \eta_i$ can be viewed as an artificial viscosity with η_i being the same as that in Eqn. (1). For the exact solution to the flow problem this additional elliptic operator is a null operator. However, in the DEVSS method, $\tilde{e}_a$ is explicitly determined by solving the following equation.

$$\tilde{e} - \tilde{e}_a = 0 \tag{6}$$

In a finite element simulation of viscoelastic flow, strain-rate tensor is discontinuous across the element boundaries, whereas a continuous interpolation is used for $\tilde{e}_a$, resulting in a non-zero value of the additional elliptic operator. In the present work, linear continuous interpolation over tetrahedral finite elements was used for $\tilde{e}_a$. The linear interpolation over tetrahedral finite elements was also used for pressure and the extra stress tensor τ_i. However, for velocity, the linear continuous interpolation over tetrahedral finite elements was augmented by an extra node at the centroid of the tetrahedral finite element. The extra node at the centroid of each tetrahedral finite element is required to satisfy the Babuska-Brezzi stability condition [10] for the incompressible flow simulation.

Coextrusion Simulation Equations

For simulation of a multilayer flow of polymers during coextrusion, the velocity and stresses are required to be continuous across the interface between the adjacent polymer layers [3]. That is,

$$\vec{u}^{(1)} = \vec{u}^{(2)} \tag{7}$$

$$\tilde{\tau}^{(1)} = \tilde{\tau}^{(2)} \tag{8}$$

$\vec{u}^{(1)}$ and $\tilde{\tau}^{(1)}$ are the velocities and stresses on one side of the interface, with $\vec{u}^{(2)}$ and $\tilde{\tau}^{(2)}$ being the velocities and stresses on the other side of the interface. Besides the continuity of velocity and stress, coextrusion simulation requires enforcement of the no-cross-flow condition at the interface. That is, the velocity component normal to the interface must be zero at every point on the interface.

$$\vec{u} \cdot \vec{n} = 0 \tag{9}$$

where $\vec{u}$ is the velocity, and $\vec{n}$ is the unit vector perpendicular to the interface.

Mesh Partitioning Technique

In the three-dimensional simulations of coextrusion reported in the literature, finite element mesh is modified after each flow simulation iteration, such that the inter-element boundaries coincide with the interface between adjacent layers of different polymers [3]. Such an approach using an interface-matched finite element mesh can only be employed for simulating a two-dimensional system or a simple three-dimensional system such as a rectangular die. For real-life coextrusion systems, with complex three-dimensional die channel geometry, repeated generation and modification of interface-matched finite element meshes is impractical.

In the present work, a three-dimensional mesh of tetrahedral finite elements was generated over the complete flow channel in the die. This finite element mesh is not modified or regenerated at any stage during coextrusion simulation. Thereby, allowing simulation of even highly complex coextrusion systems.

In the mesh partitioning technique which is employed in this work, the interface between adjacent layers of different polymers is represented by a surface mesh of linear triangular finite elements. However, the surface mesh of triangular elements on the interface and the three-dimensional mesh of tetrahedral elements in the coextrusion die are completely independent of each other. This decoupling between the two finite-element meshes is possible because in the mesh partitioning technique for coextrusion simulation, the interface between adjacent polymer layers is not required to match with the inter-element boundaries in the three-dimensional mesh of tetrahedral finite elements. Instead, in the software used in this work, the interface is allowed to pass through the interior of the tetrahedral finite elements in the three-dimensional mesh.

In the mesh partitioning technique for coextrusion simulation the tetrahedral elements which are intersected by the mesh of triangular elements on the interface are partitioned into two tetrahedral, pyramidal, or prismatic finite elements. Further details of the mesh partitioning technique are available in our earlier publications [4, 11].

Materials

For the bi-layer flow presented in this paper, Giesekus model parameters given below were used for the two different grades of polystyrenes [5].

Styron 472:

$\eta_s = 48.4$ Pa. s, $\eta_1 = 1.383 \times 10^3$ Pa. s

$\lambda_1 = 2.0 \times 10^{-2}$ s, $\alpha_1 = 0.4$

Styron 678E:

$\eta_s = 26.4$ Pa. s, $\eta_1 = 5.278 \times 10^2$ Pa. s

$\lambda_1 = 1.0 \times 10^{-2}$ s, $\alpha_1 = 0.4$

The experimental data for the viscosities of the two polystyrenes [3], along with the fit to the experimental data using the Giesekus model parameters given above [5], is shown in Fig. 1. It is evident from Fig. 1 that the viscosity of Styron 472 is much higher than that of Styron 678E.

Bi-layer Coextrusion in a Square Channel

One of the main motivations for including viscoelastic effects in coextrusion simulation in this work was to be

able to capture encapsulation of one polymer by another polymer which is often observed in polymer coextrusion. For instance, Karagiannis et al. [3] obtained the experimental data on encapsulation of Styron 472 by Styron 678E in a bi-layer flow in a square channel. Karagiannis at el. [3] observed that starting with a straight interface shape at the contact line, where the two polymers meet for the first time, Styron 678E progressively encapsulated Styron 472 as the two polymers flowed side-by-side in the square channel (Fig. 2). However, no such encapsulation was obtained in their simulation of the bi-layer flow using a purely viscous generalized Newtonian formulation (Fig. 3). Similar simulation of bi-layer flow in a square channel using a purely viscous formulation performed in our earlier work [4] could not capture the encapsulation observed in experiments.

It was reported by Sunwoo et al. [5] that they could capture the encapsulation of Styron 472 by Styron 678E when they included viscoelastic effects in the simulation, which was the main motivation for including the viscoelastic effects in coextrusion simulation in this work. Sunwoo et al. [5] reported that the predicted encapsulation in their simulation of the bi-layer flow was the largest and the closest to the experiments when a large value of the parameter $\alpha_i = 0.4$ in Eqn. 1 was used in the simulation. Therefore, in the present work, the same Giesekus model parameters with $\alpha = 0.4$, as those employed by Sunwoo et al. for Styron 472 and Styron 678E (given above) were also used in the present work to simulate the bi-layer flow in the square channel. The simulation results thus obtained are presented next in this section.

To characterize the flow, a non-dimensional shear rate (Deborah number, De) is defined as

$$De = \frac{3U}{b}\lambda_0 \qquad (10)$$

where U is the average velocity in the square portion of the flow channel, b is the half of the square cross-section side length, and λ_0 is characteristic relaxation time of the polymer at low shear rate.

$$\lambda_0 = \frac{\sum_{i=1}^{N}\eta_i\lambda_i}{\eta_s+\sum_{i=1}^{N}\eta_i} \qquad (11)$$

To define the Deborah number for the bi-layer flow in the square channel, the average value of the characteristic relaxation time, λ_0, for the two fluids employed was used. For the average velocity in the square channel required for a specified Deborah number, the appropriate value of the uniform velocity was specified at the entrances of the two polymers, whereas all components of the extra stress tensor were specified to be zero at the entrances. Zero velocity was enforced at the die walls.

For $De = 1$, with Styron 472 in the lower layer and Styron 678E in the upper layer, the axial velocity distribution for the bi-layer flow in the square channel is shown in Fig. 4. Beyond $De = 1$ simulation of the bi-layer flow did not converge. Starting with the same uniform velocity at the entrances of the two polymers, after the two polymers meet the velocity slowly increases as the two polymers go through the converging portion of the channel, and the highest velocity is obtained once the two polymers reach the square portion of the channel. The velocity then remains relatively unchanged as the two polymers flow through the square channel

The transverse velocity distribution due to secondary flow in the bi-layer coextrusion in the square channel for $De = 1$ is shown in Fig. 5. For the bi-layer flow, in Fig. 5 there are eight recirculating vortices. However, in contrast to the eight vortices in flow of a single polymer, which have the same size, the vortices for the bi-layer flow in Fig. 5 have different sizes. For instance, in Fig. 5 the two vortices at the bottom are significantly smaller than the two vortices just above the two bottom vortices. Also, in contrast to the vortices for flow of a single polymer, for the secondary flow in Fig. 5 there is no stagnation region in the middle of the square cross-section. Instead, near the center of the square cross-section the fluid from the bottom vortices is entering into the flow in the two vortices on top.

The shape of the interface between the two polymer layers for $De = 1$ is shown in Fig. 6 (a). The corresponding final shape of interface at the exit of the square channel is shown in Fig. 6 (c). Starting with a straight line interface shape at the contact line, where the two polymers meet for the first time, the interface in Fig. 6 (a) starts to wave upwards near the middle and near the two ends with troughs in between, resulting in the W-shaped interface at the die exit in Fig. 6 (c). In contrast to the wavy interface shape in Fig. 6 (a) and 6 (c), for $De = 0.1$ in Figs. 6 (b) and 6 (d), the predicted interface shape just has a slight curvature but does not have a wavy shape. For $De = 0.1$ the elastic effects in the flow, and hence, the secondary flow vortices are negligible, resulting in the simple shape of the interface which is similar to the interface shape obtained in a purely viscous simulation by Karagiannis et al. [3].

The magnitude of the second normal stress difference, $|\tau_{22} - \tau_{33}|$, for the bi-layer flow for $De = 1$ is shown in Fig. 7. The magnitude of the second normal stress difference, which results in the secondary flow vortices observed in Fig. 4, is the maximum near the middle of each of the four sides of square cross-section, and is zero near the center of the cross-section, and is also zero along the two diagonals of the square cross-section.

The pressure variation for the bi-layer flow in square channel is shown in Fig. 8. As expected, the pressure is zero at the exit and increases towards the two entrances. Also, for the same velocity at the entrances of the two polymers, the pressure gradient is higher in the narrower feed channel of the upper layer.

Discussion

It should be noted that in contrast to the results reported by Sunwoo at el. [5], no encapsulation of Styron 472 by Styron 678E was obtained in Figs. 6 (a) and (c). For encapsulation, in Figs. 6 (a) and (c) the interface

between the two layers should have bent downwards near the two walls. Instead, in Figs. 6 (a) and (c), near the two side walls the interface is bent upward, which is caused by the secondary flow vortices shown in Fig. 4. Sunwoo at el. [5] did not show the structure of secondary flows in their simulation. Therefore, it is difficult to interpret how Sunwoo et al. [5] could have obtained the encapsulation in the bi-layer flow using the Giesekus model parameters given in Section 3. Since encapsulation was not obtained for lower Deborah number in Fig. 6 (b) and (d), where the elastic effects are negligible, and no encapsulation was obtained in purely viscous simulation of the flow in the literature [3, 4], the encapsulation phenomena is also not caused solely by the difference in the viscosity of the two polymers.

At this point, we believe that polymer encapsulation in coextrusion is a surface phenomenon, which is caused by the difference in the wettability (spreading tendency of the polymer on die surface) and surface tension of the two polymers used. The polymer with higher wettability is expected to encapsulate the other polymer during coextrusion.

Conclusions

The Giesekus model was used for viscoelastic simulation of a bi-layer flow in a square coextrusion die. In contrast to the findings reported in the literature, in the present work even with viscoelastic effects included in the simulation, encapsulation of a high viscosity polymer by a lower viscosity polymer, which is often observed in coextrusion experiments, could not be captured. Since the viscous encapsulation could not be captured with a purely viscous formulation in our earlier work, and similar work by other groups in the literature, it is concluded that encapsulation is not caused by viscous or viscoelastic effects. Instead, it is concluded that difference in wettability and surface tension of the two polymers is probably the major factor contributing to the encapsulation phenomenon.

References

1. C. Rauwendaal, "Polymer Extrusion", 4th Edition, Hanser Publishers, (2001).
2. J. Dooley and L. Rudolph, *J. of Plastic Film and Sheeting*, Vol. 19, 111 – 122 (2003).
3. A. Karagiannis, A. N. Hyrmak, and J. Vlachopoulos, *Rheologica Acta*, Vol. 29, 71 – 87 (1990).
4. M. Gupta, *SPE ANTEC Technical Papers*, Vol. 54, 217 – 222 (2008).
5. K. B. Sunwoo, S. J. Park, S. J. Lee, K. H. Ahn, and S. J. Lee, *Rheologica Acta*, Vol. 41, 144 – 153 (2002).
6. R. G. Larson, "Constitutive Equations for Polymeric Melts and Solutions", Butterworths, Boston, MA, (1988).
7. J. N. Reddy, "An Introduction to Finite Element Method", 3rd Ed., McGraw Hill, (2006).
8. A. N. Brooks and T. J. R. Hughes, *Computer Methods in Applied Mechanics and Engineering*, Vol. 32, 199 – 259 (1982).
9. R. Guienette and M. Fortin, *J. of Non-Newtonian Fluid Mechanics*, Vol. 60, 27 – 52 (1995).
10. T. Coupez and S. Marie, *International Journal for Supercomputer Applications and High Performance Computing*, Vol. 11, 277 – 285 (1997).
11. M. Gupta, *SPE ANTEC Technical Papers*, Vol. 56, 2032 – 2036 (2010).

Acknowledgement

This work was supported by the grant # 1046495 from the National Science Foundation.

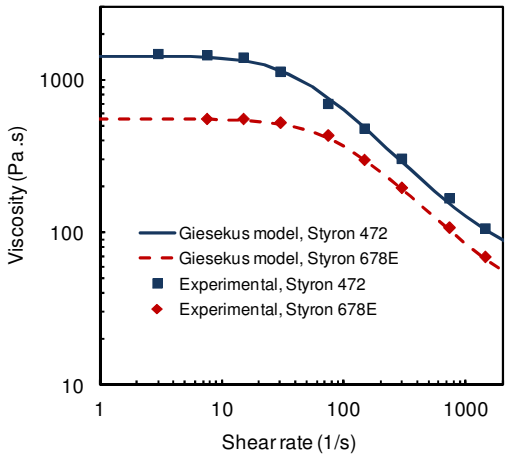

Fig. 1 Viscosity of the two polystyrenes.

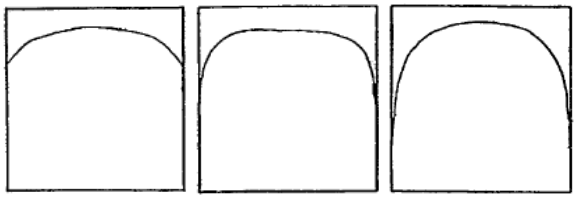

Fig. 2 Interface shape in the experiments. The distance from the square entrance is (a) 0.4 *L*, (b) 2.42 *L*, and (c) 6.71 *L*, with *L* being the length of the side of the square [3].

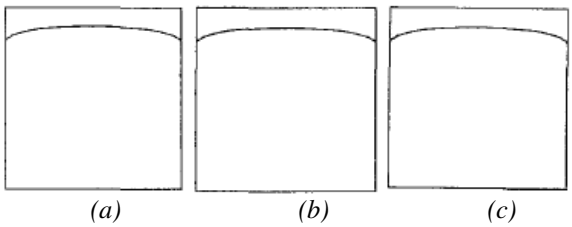

Fig. 3 Interface shape predicted by a purely viscous simulation. The distance from the square entrance is (a) 0, (b) 0.42 *L*, and (c) 2.42 *L*, with *L* being the length of the side of the square [3].

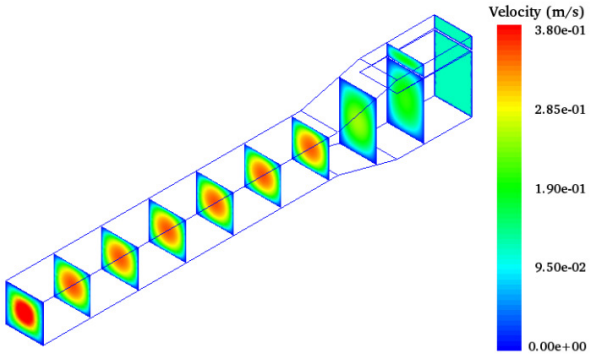

Fig. 4 Axial velocity distribution in a bi-layer flow in a square channel for $De = 1$.

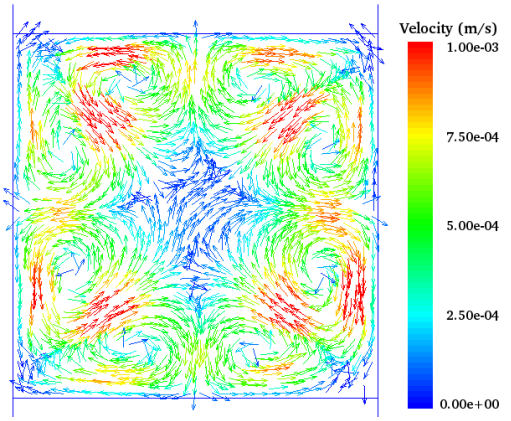

Fig. 5 Secondary flow vortices in a bi-layer flow in a square channel for $De = 1$.

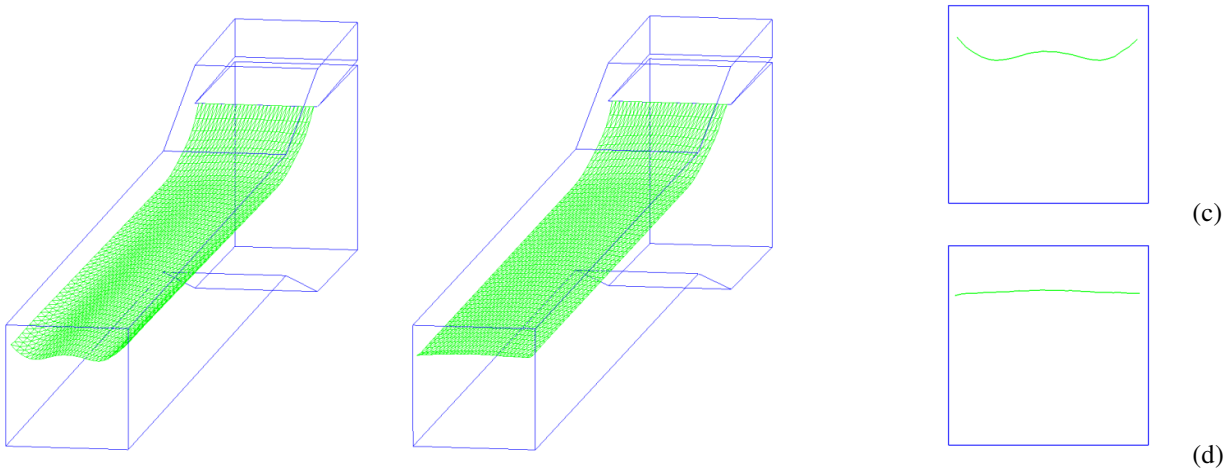

Fig. 6 Shape on the interface in a bi-layer coextrusion in a square channel. Interface shape for (a) De $= 1$, (b) De $= 0.1$. Interface shape at channel exit for (c) $De = 1$, (d) $De = 0.1$.

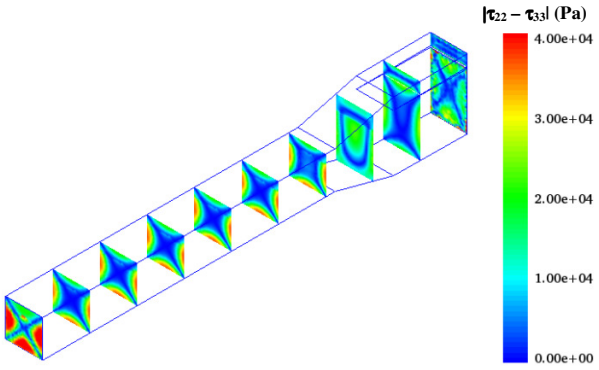

Fig. 7 Magnitude of the second normal stress difference in a bi-layer flow in a square channel for $De = 1$.

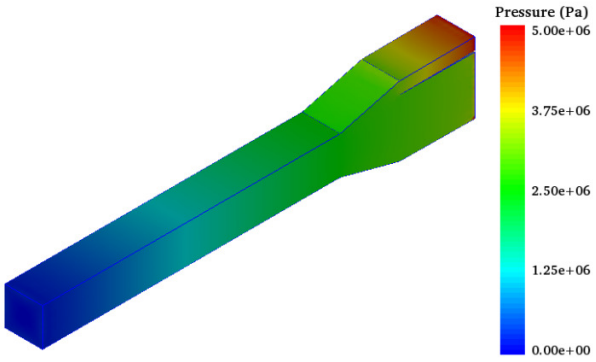

Fig. 8 Pressure distribution in a bi-layer flow in a square channel for $De = 1$.